frontiers in Earth Science

BRIEF RESEARCH REPORT
published: 23 August 2021
doi: 10.3389/feart.2021.680180

Asian Winter Monsoon Imprint on the Water Column Structure at the Northern South China Sea Coast

Yancheng Zhang[1,2], Kai Zhu[2], Chao Huang[3,4], Deming Kong[4], Yuxin He[5], Huanye Wang[6], Weiguo Liu[6], Zhouqing Xie[7], Gangjian Wei[3] and Zhonghui Liu[2]*

[1]School of Marine Sciences, Sun Yat-sen University, Zhuhai, China, [2]Department of Earth Sciences, The University of Hong Kong, Hong Kong, China, [3]State Key Laboratory of Isotope Geochemistry, Guangzhou Institute of Geochemistry, Chinese Academy of Sciences, Guangzhou, China, [4]Guangdong Province Key Laboratory for Coastal Ocean Variation and Disaster Prediction, Guangdong Ocean University, Zhanjiang, China, [5]School of Earth Sciences, Zhejiang University, Hangzhou, China, [6]State Key Laboratory of Loess and Quaternary Geology, Institute of Earth Environment, Chinese Academy of Sciences, Xi'an, China, [7]Anhui Key Laboratory of Polar Environment and Global Change, Department of Environmental Science and Engineering, University of Science and Technology of China, Hefei, China

OPEN ACCESS

Edited by:
Shengfa Liu,
Ministry of Natural Resources, China

Reviewed by:
Kefu Yu,
Guangxi University, China
Hong Yan,
Institute of Earth Environment (CAS), China
Qian Li,
Qingdao National Laboratory for Marine Science and Technology, China

***Correspondence:**
Yancheng Zhang
zhangych99@mail.sysu.edu.cn

Specialty section:
This article was submitted to Quaternary Science, Geomorphology and Paleoenvironment, a section of the journal Frontiers in Earth Science

Received: *13 March 2021*
Accepted: *12 July 2021*
Published: *23 August 2021*

Citation:
Zhang Y, Zhu K, Huang C, Kong D, He Y, Wang H, Liu W, Xie Z, Wei G and Liu Z (2021) Asian Winter Monsoon Imprint on the Water Column Structure at the Northern South China Sea Coast. Front. Earth Sci. 9:680180. doi: 10.3389/feart.2021.680180

Coastal regions of the northern South China Sea (SCS) strongly interact with the Asian monsoon circulation (AMC). Thus, variations of sea surface temperature (SST) here are newly suggested to document AMC changes in an effective manner, but additional physical parameters of oceanic conditions, probably also in relation to the AMC system, remain poorly understood. In this study, we analyzed glycerol dialkyl glycerol tetraethers (GDGTs) from a well-dated sediment core YJ, retrieved at the northern SCS coast, to further scrutinize the intrinsic response of water column to winter AMC strength. It shows that within the time frame of past ~1,000 years, the tetraether index of lipids with 86 carbon atoms (TEX_{86}) and published alkenone ($U^{K'}_{37}$) temperature records together confirm a reduced thermal gradient during the Little Ice Age (LIA), in comparison to that during the Medieval Climate Anomaly (MCA). Considering concurrent variations of the branched and isoprenoid tetraether (BIT) and the ratio of archaeol to caldarchaeol (ACE), for example, with decreased values (<~0.3) for the former and relatively high values for the latter at the LIA, indicative of stratification and salinity changes, respectively, these multiple lines of evidence thereby call for well mixing of onsite water at site YJ correspondingly. Our results suggest that winter AMC strength is a critical factor for mixing subsurface waters and modifying thermal/saline conditions at the northern SCS coasts through the last millennium and also, perhaps, on longer timescales.

Keywords: South China Sea, coastal conditions, GDGTs, last millennium, Asian winter monsoon

INTRODUCTION

The Asian monsoon circulation (AMC), as triggered by large-scale thermal contrast between ocean and land, characterizes a seasonal reversal of prevailing wind directions. In the summertime, it carries an enormous amount of moisture from the Indian and Pacific Oceans toward southern and northeastern Asia, and, consequently, exerts a considerable influence over the water cycle and the terrestrial ecosystem (Wang et al., 2017; Zhang et al., 2017). In this regard, much attention has been drawn until now to explore summer AMC variability and the physical mechanism(s) from seasonal to orbital timescales (e.g., Hu et al., 2008; An et al., 2011; Liu et al., 2015; Xie et al., 2015;

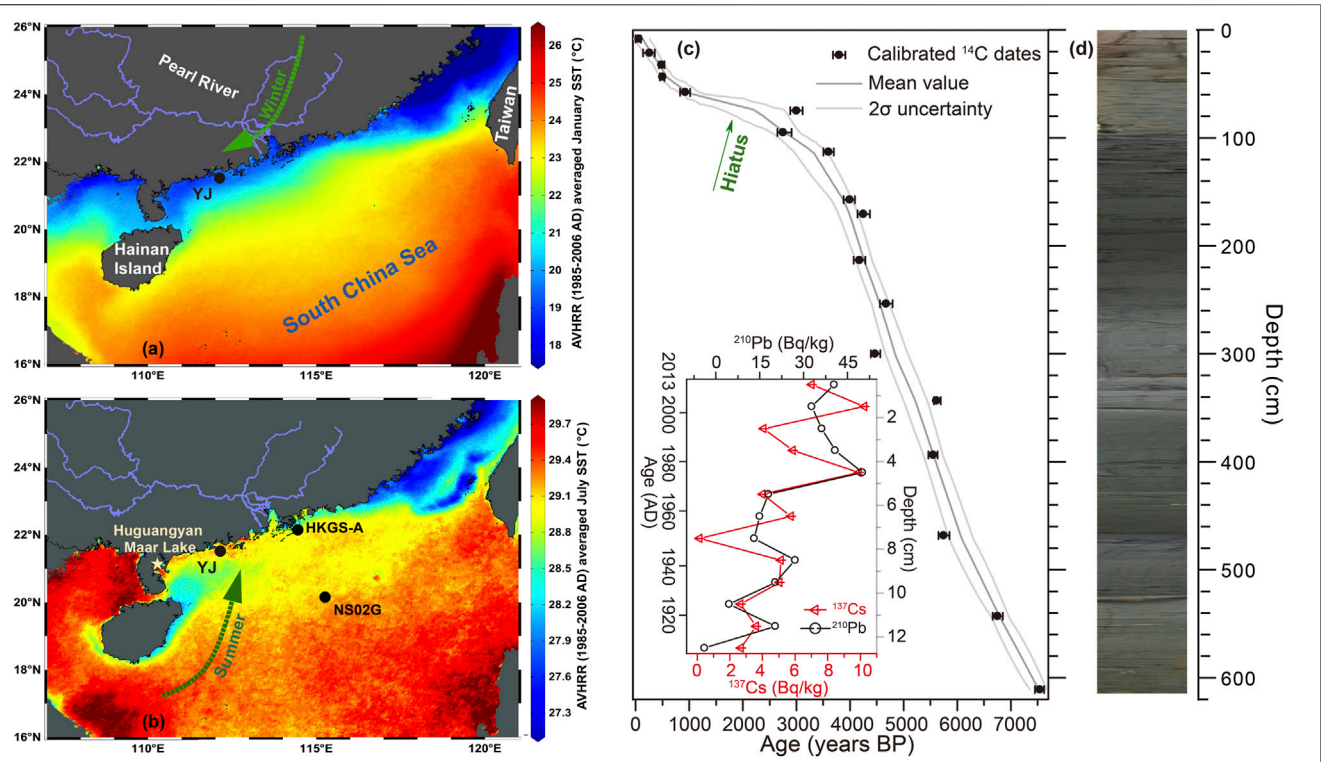

FIGURE 1 | Regional setting and the site of core YJ, existing paleorecords in the northern South China Sea (black dots) and at Huguang Maar Lake (orange star) as mentioned in the main text, are plotted against long-term (1985–2006 AD) averaged January **(A)** and July **(B)** sea surface temperature (SST, color scale) from the AVHRR dataset (Casey, 2013). Chronology **(C)** and lithology **(D)** of core YJ are cited from Huang et al. (2018) and Zhang et al. (2019). Note that the core-top **(C)** is calculated based on ^{210}Pb/^{137}Cs dates, to be 2013 AD when our core YJ was retrieved.

Cheng et al., 2016). In contrast, the winter component of the AMC itself often diverges cold-dry air from the Asian countries such as Siberia-Mongolia toward oceans, thus with little potential to deliver water vapor directly. Despite such fact, winter AMC is still of importance in transporting eolian dust and/or aerosol, and therefore in regulating the regional (and global) climate system (Maher et al., 2010; Kok et al., 2018). Combined with its impact upon the summer AMC precipitation subsequently (Bollasina et al., 2011; Li et al., 2016; Cai et al., 2019), a complete understanding of winter AMC variations at present and, if possible, before the instrumental era (after ~1850 AD) (e.g., Wen et al., 2016; Kang et al., 2020) would provide constructive insight into their intrinsic link against both anthropogenic and natural backgrounds. Abundant analyses based on the grain size and geochemical proxies from Chinese loess sequences at available sparse sites (Stevens et al., 2007; Li and Morrill 2015), on the one hand, have indeed advanced our knowledge about this topic, but on the other hand, these paleorecords, distributed across continental interiors, rather face difficulty to draw a clear picture of winter AMC behavior, for example, its far-field effect on terrestrial ecosystem especially. For example, at Huguangyan Maar Lake, winter AMC intensity, as inferred from diatom assemblages (Wang et al., 2012) and magnetic susceptibility (Yancheva et al., 2007), respectively, presents controversial temporal features during the Holocene (since ~11,700 years ago before present, "yr BP" hereafter).

Next to Huguangyan Maar Lake, the South China Sea (SCS) is also strongly involved into the AMC coupling process (e.g., Xie et al., 1998; Lau and Nath 2009; Wang et al., 2009; Liu and Zhu 2016) and hence well suited to fingerprint its variability. In fact, along the SCS northern coasts, sea surface temperature (SST) apparently exhibits shore-parallel gradient and intensive vertical mixing in winter, while horizontal homogenization and vertical stratification in summer (**Figures 1A,B**; Wang, 2007; Jing et al., 2009). Such seasonality of SST variations and their difference, for example, at both horizontal and vertical scales, are readily capable of revealing winter AMC signals across different timescales (e.g., Tian et al., 2010; Huang et al., 2011; Steinke et al., 2011; Kong, 2014a, Kong et al., 2014b). Particularly, our recent study (Zhang et al., 2019), based on a well-dated sediment core YJ, ~200 km far away from the Pearl River delta (**Figure 1**), has shown extraordinary decrease (by up to ~4°C) of alkenone SSTs and remarkable increase (by two to four orders of magnitude) of wind-borne terrigenous hopane contents during the Little Ice Age (LIA, ~150–550 years BP), consequently demonstrating an overall intensification of winter AMC, relative to the Medieval Climate Anomaly (MCA, ~700–1,100 years BP) and other intervals in the context of Holocene. This explanation, albeit well corroborated by a growing number of terrestrial paleorecords (e.g., Yancheva et al., 2007; Kang et al., 2020), still deserves independent evidence of oceanic conditions which, as inherently linked to SST change, would offer excellent

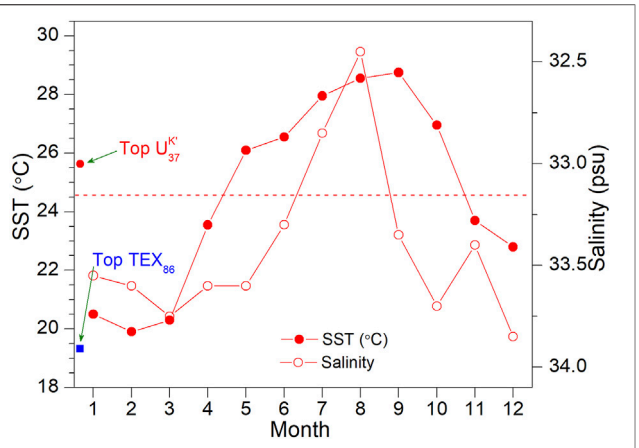

FIGURE 2 | Comparison between temperature estimates at the topmost sample based on $U^{K'}_{37}$ and TEX_{86} proxies, respectively. Observational SSTs and salinity near the core site (112.125°N, 21.625°E, Casey, 2013; Zweng et al., 2013) are also shown. The dashed line represents the annual mean SST value.

opportunity to further illustrate the fundamental role of winter AMC variations in affecting coastal waters. To this end, the time window of last millennium covering both the LIA and MCA, two well-identified climate anomaly intervals during the late Holocene (Mann et al., 2008), is specifically focused here for a tentative attempt to examine how the northern SCS coastal conditions, for example, in terms of both salinity and thermal properties, would have responded to winter AMC change at multi-centennial timescales.

Taking the advantage of sediment core YJ, including i) high-quality control of the chronological framework (**Figures 1C,D**) and ii) limited influence of the Pearl River freshwater discharge (**Figure 2**), we hence directly analyzed glycerol dialkyl glycerol tetraether (GDGT) lipid biomarkers on its uppermost ~65 cm section. Together with the existing measurements of the alkenone unsaturation index ($U^{K'}_{37}$, see definition in Prahl et al., 1988) and hopane components, as earlier reported by Zhang et al. (2019), this study aimed to investigate the hydrological properties of the onsite water column. We hereby present proxy records of the ratio of archaeol to caldarchaeol (ACE), the branched and isoprenoid tetraether (BIT), respectively, and the tetraether index of lipids with 86 carbon atoms (TEX_{86}) over the past ~1,000 years. These results, although potentially associated with various parameters in view of their original interpretations, are utilized to manifest salinity (Turich and Freeman 2011; Wang et al., 2013), stratification (Yamamoto et al., 2013; Wang et al., 2021), and integrated temperature of the whole water column (Xing et al., 2015; Wei et al., 2020), respectively. On this basis, the difference of our paired $U^{K'}_{37}$-TEX_{86} values, a rough measure of vertical thermal gradient, could be used to infer the water column structure changes induced by the winter AMC. Overall, this study helps clarify the dynamical interplay between winter AMC strength and northern SCS coastal conditions throughout the last millennium and, as a result, evoke a careful consideration of regional environmental settings in properly interpreting proxy-based temperature signals.

MATERIAL AND METHODS

Core Site and Chronology

Geographically, sediment core YJ (112°8.08′ E, 21°31.44′ N) is raised at a water depth of ~21 m from the inner continental shelf offshore Yangjiang city with a distance of ~200 km to the southwest of the Pearl River estuary. This site, according to modern observations (e.g., Dunn and Ridgway 2002; Casey, 2013), characterizes prominent SST variations between ~28.3°C in summer (June-July-August, JJA) and ~20.9°C in winter (December–January–February, DJF), but small changes in sea surface salinity (i.e., ~32.4 psu in JJA and ~33.4 psu in DJF; **Figure 2**) due to limited influence of the Pearl River discharge. Most importantly, it is located at the coastal sector outside ~1°C cooling effect of summer upwelling (e.g., to the east of the Pearl River delta and northeast of the Hainan Island, **Figure 1B**), while surface cooling here is largely determined by vertical mixing of the onsite water column in winter (**Figure 1A**). This site is hence well suited to examine the response of northern SCS coastal conditions to winter AMC changes, for example, by using the $U^{K'}_{37}$ SST record in our previous study (Zhang et al., 2019).

The age model of this core, as already published before by Huang et al. (2018) and Zhang et al. (2019), was achieved by combining both lead (^{210}Pb)/cesium (^{137}Cs) and radiocarbon (^{14}C) methods. To summarize, measurements of 13 ^{210}Pb/^{137}Cs radionuclide activity and 18 ^{14}C dates (at Beta Analytic Inc., United States) were implemented on samples of bulk sediments above 13 cm and complete shells below this depth, respectively. These age control points were then operated within R script BACON software (version 2.2, Blaauw and Christen 2011) and the Marine 13 calibration curve (Reimer et al., 2013), using default parameters and a 252-year correction of regional reservoir age (Southon et al., 2002; Yu et al., 2010), to compute the mean age and 2σ uncertainty at 1 cm resolution. Such a chronological framework hints a possible hiatus of sedimentary deposit at the depth between ~65 and 85 cm (**Figure 1C**; see details in Zhang et al., 2019). Hence, we mainly focus on the topmost 65 cm of the core YJ, roughly spanning the past ~1,000 years, to analyze GDGT biomarkers for detecting the AMC signal across the LIA and MCA.

Organic Biomarkers

Core YJ was sampled continuously with a step of 1 cm down its uppermost 65 cm, which, based on our chronology as stated in *Core Site and Chronology* section, guaranteed a temporal resolution of ~10–15 years per sample for the past ~1,000 years. Afterward, bulk sediment samples (~5 g) were freeze-dried, then grounded, and soaked to extract total lipids by solvent dichloromethane (DCM): methanol (MeOH) (9:1; v/v) in 60 ml vials, under an ultrasonic wave in the 40°C water bath for three cycles (~15 min each). The extract was subsequently hydrolyzed with 6% KOH in MeOH to remove alkenoates and separated into three fractions *via* silica gel column chromatography with successive eluents of *n*-hexane, DCM,

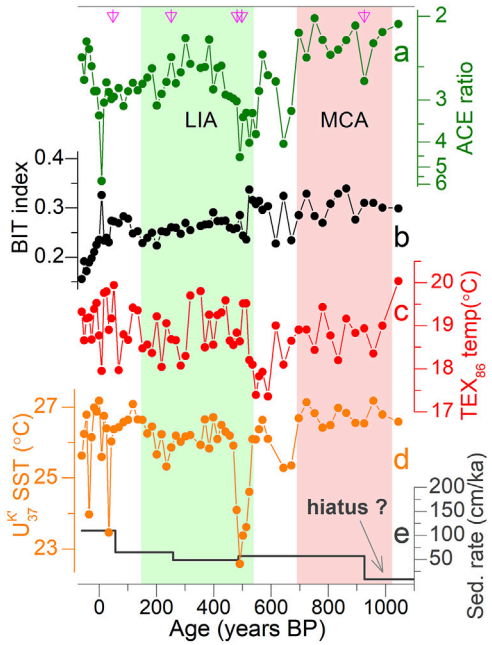

FIGURE 3 | GDGT proxies of sediment core YJ during the last millennium, for example, **(A)** ratio of archaeol to caldarchaeol (ACE) (higher values downward), **(B)** the branched and isoprenoid tetraether (BIT), **(C)** TEX_{86}-based temperatures, **(D)** $U^{K'}_{37}$-SST record, and **(E)** sedimentation rates (Zhang et al., 2019). Color bars outline the Little Ice Age (LIA, ~150–550 years BP) (green) and Medieval Climate Anomaly (MCA, ~700–1,100 years BP) (red), and triangles denote ^{14}C age control points.

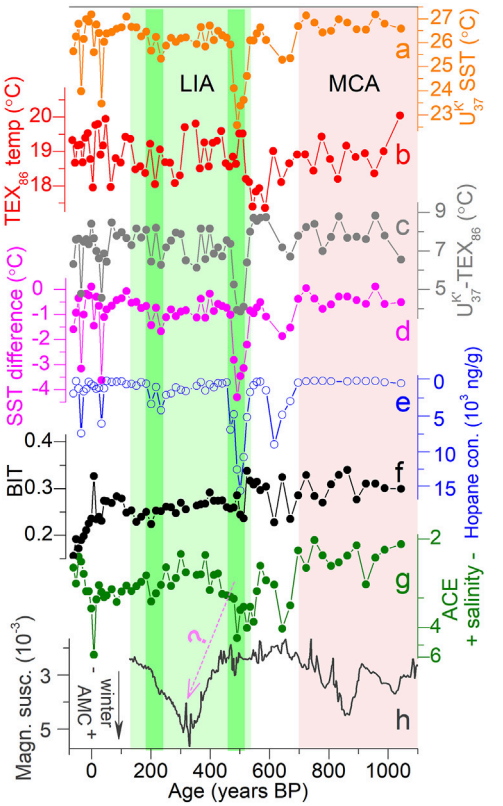

FIGURE 4 | Organic geochemical proxies of core YJ over the last millennium, including **(A)** $U^{K'}_{37}$-SST record (Zhang et al., 2019), **(B)** TEX_{86}-based temperature, **(C)** vertical thermal gradient at site YJ ($U^{K'}_{37}$ – TEX_{86} values), **(D)** $U^{K'}_{37}$-SST difference between two sites YJ and NS02G (YJ minus NS02G), **(E)** hopane compounds (Zhang et al., 2019), **(F)** the branched and isoprenoid tetraether (BIT), and **(G)** the ratio of archaeol to caldarchaeol (ACE). Note that magnetic susceptibility at Lake Huguangyan Maar (higher values downward, Yancheva et al., 2007) is also plotted **(H)** for comparison (with a possible shift of their peaks due to the age uncertainty). Color bars mark the same intervals as in **Figure 3** (two cold epochs within the LIA, e.g., ~250 years BP and ~500 years BP, are further highlighted).

and MeOH, respectively. Finally, GDGTs were isolated in MeOH fraction, alkenones in DCM fraction, and *n*-alkanes in hexane fraction.

Analyses of MeOH fraction were conducted on high-performance liquid chromatography atmospheric pressure chemical ionization (HPLC-APCI)-mass spectrometry (e.g., Liu et al., 2013). An aliquot of the fraction was directly dried under N_2, and then redissolved in hexane: isopropanol (99:1; v/v) and filtered after mixing with a known amount of C_{46} internal standard (Huguet et al., 2006). Selected ion monitoring (SIM), which targets specific mass numbers for GDGT components (membrane lipids biosynthesized as multiple homolog series of isoprenoid or methyl-branched isomers, termed isoprenoid-GDGTs, and branched-GDGTs, respectively, see detailed description in Schouten et al., 2013), was used to enhance the detection sensitivity. Quantification was carried out by integrating the peak area of $[M + H]^+$ ions in the extracted ion chromatogram and comparing with the C_{46} internal standard. We then calculated the ACE, BIT, and TEX_{86} indices using equations as given below:

$$ACE = \frac{archaeol}{archaeol+caldarchaeol\times10} \times 100$$ (Turich and Freeman 2011; Wang et al., 2013),

$$BIT = \frac{I+II+III}{I+II++III+cren}$$ (Hopmans et al., 2004),

$$TEX_{86} = \frac{GDGT_2+GDGT_3+cren'}{GDGT_1+GDGT_2+GDGT_3+cren'}$$ (Schouten et al., 2002).

TEX_{86} values were then converted to temperature estimates, using the calibration equation: SST = 68.4 ×log (TEX_{86})+38.6 (Kim et al., 2010). Analytical uncertainties for our laboratory standards are typically less than 5% for the BIT and ACE values and 0.01 unit for TEX_{86}.

RESULTS

Throughout the past millennium, ACE values appear to be relatively high during the LIA, especially at its onset (centered around ~500 years BP), as compared to the MCA (**Figure 3A**). In contrast, the BIT index generally experiences a gradual declining trend from ~0.3 during the MCA (and the earlier epochs, marked by a possible hiatus in sediment accumulation and hence not shown here) toward ~0.15 in the recent years (**Figure 3B**). Unlike these two modes, TEX_{86}-based temperatures, although fluctuated

within a large range (nearly about 3°C in terms of magnitude, **Figure 3C**), are apparently trendless over the investigated interval. However, when placed together with the existing $U^{K'}_{37}$-based SST record of the same core YJ (**Figures 3D,E**), there exists certain similarity in the overall temporal patterns between SST (despite a substantial cooling of up to ~4°C, Zhang et al., 2019) and TEX_{86} temperatures over the LIA (e.g., increase at the first half and decrease at the second half), but for the MCA, variations of these two independent records are clearly featured by different structures. Collectively, the LIA interval characterizes increase in ACE values and wind-borne hopane compounds (Zhang et al., 2019), and decrease in BIT ratios, SST, and vertical temperature gradient ($U^{K'}_{37}$ – TEX_{86}values), relative to those during the MCA (**Figure 3** and **Figure 4**).

DISCUSSION

Recent studies have shown that the possible source of brGDGTs, for example, terrigenous originated (e.g., soil) or *in situ* synthesized (mainly at subsurface waters), is critical to determine the BIT index and thus its proper explanation (Weijers et al., 2014; Xiao et al., 2016; Wang et al., 2021). For example, more subsurface production of brGDGTs in the Qiongzhou Strait is suggested to be responsible for higher BIT values (~0.4–0.6), which, as a result, reflect enhanced stratification of the onsite water column and thus change in summer AMC strength (Wang et al., 2021). At our study site YJ, BIT values, primarily subjected to crenarchaeol (one major component of isoGDGTs) rather than brGDGT variations (**Supplementary Figure 1**), also imply water column stratification. A set of field surveys, based on collection of both the sediment trap and core-top samples, show that, at the transition zones between the Pearl River estuary and the SCS northern coast, the bloom of autotrophic ammonia-oxidizing *Thaumarchaeota*, main producers of isoGDGTs with limited brGDGTs, tends to preferably occur under the hydrological conditions in the coldest months, like low light levels (e.g., Zhang et al., 2013; Wang et al., 2015; Jia et al., 2017) and less stratified water. Meanwhile, at normal marine settings, including those on the continental shelf, light and redox conditions can also yield redistribution of *Euryarchaeota*/*Archaea* community, leading to stratification of archaeal membrane lipids (with relatively high archaeol in subsurface waters, Turich et al., 2007; Weijers et al., 2014; Xiao et al., 2016; Zhu et al., 2016). In this sense, the coeval variations of isoGDGTs and archaeol abundance in our particular case may cause opposite temporal patterns of BIT and ACE indices (**Supplementary Figures 1, 2**). This fact, in contrary to a recent study presented by Wang et al. (2021) who have applied the concomitant increase in these two proxies to represent enhanced stratification of the northern SCS coastal water, thereby calls for other interpretation(s) to reconcile competing patterns of our BIT and ACE proxies (**Figures 3A,B**). Considering the small variations of BIT values and brGDGTs (**Supplementary Figure 1**), we thus interpret relatively low BIT ratios during the LIA as increased production of the ubiquitous *Thaumarchaeota*, relative to other *Euryarchaeota*/*Archaea*. Besides, it is also worth stressing that despite similar features of changes in crenarchaeol and caldarchaeol (GDGT-0) (**Supplementary Figures 1, 2**), two most abundant components of isoGDGTs, the observed ACE values here may still primarily respond to *Euryarchaeota*/*Archaea* community changes, therefore no longer being an indicator of water column stratification (e.g., Wang et al., 2021).

Based on the results of previous studies (Turich and Freeman, 2011; He et al., 2020), the ACE index might represent salinity if it mainly responds to *Euryarchaeota*/*Archaea* community changes. This prerequisite indeed exists in our case, because one could apparently see a major control of *Euryarchaeota*/*Archaea* on the ACE record (**Supplementary Figure 2**). Due to the different characteristics of BIT and ACE records that strongly exclude the latter as a tracer of stratification (Wang et al., 2021), we instead assume ACE to manifest salinity. As such, multi-centennial–scale variations in our ACE record, as depicted in **Figure 4G**, suggest increased (decreased) salinity of the onsite water column across the LIA (MCA) (Turich and Freeman, 2011). Together with the inference of the available $U^{K'}_{37}$-SST record and wind-borne hopane contents, as earlier reported (**Figures 4A,E**), relatively saline conditions at our site, although only qualitatively estimated (if also taking into account the small range of vertical salinity gradient, **Figure 2**), took place along with an intensification of winter AMC strength during the LIA, and *vice versa* for the MCA. Indeed, observational datasets confirm that, on seasonal timescales, there is a homogeneous structure of *in situ* salinity and temperature changes in winter (i.e., ~33.4 psu and ~20°C down the entire water column, respectively, **Supplementary Figure 3**), relative to those in summer (i.e., ~32.4 psu/28.3°C at surface and ~33.4 psu/27.1°C at ~10–15 m water depth; Zweng et al., 2013). In analogy with this scenario, it is possible that a stronger winter AMC during the LIA would have promoted vertical mixing of the onsite water column which; as a result, it would have brought more cold waters and production of (halophilic) *Euryarchaeota*/*Archaea* community (archaeol, the major driver of ACE values) at the subsurface layers toward upward, thereby decreasing SSTs while increasing its salinity. Notably, during the LIA cold interval, a less input of riverine discharge like the Pearl River drainage, due to the concomitant reduction of summer AMC intensity, as effectively corroborated by a growing body of compelling and independent evidence (e.g., Dykoski et al., 2005; Wang et al., 2005; Zhang et al., 2008; Wang et al., 2012; Lee et al., 2019), may have also somewhat contributed to the inferred salinity increase here. Because these two processes are naturally coupled together from a climatological perspective, it is still difficult to assuredly claim which should play a major role in driving the higher salinity during the LIA. Still, an in-depth examination of winter (*via* mixing of subsurface waters) and/or summer (*via* decrease of riverine discharge) AMC impact on *in situ* salinity will need additional work in the future, for example, model simulations in particular. Regardless, variations in

winter AMC strength, as inferred from both magnetic susceptibility at Huguangyan Maar Lake (Yancheva et al., 2007) (**Figure 4H**), the $U^{K'}_{37}$ SST record and wind-borne hopane contents at site YJ, are strongly suggested to modulate the water column structure at the SCS northern coasts, for example, by superimposing additional cooling effect on the top of the LIA cold climate background (Zhang et al., 2019).

The physical mechanism for our inference is further substantiated by the BIT index and TEX_{86}-derived temperature records (**Figures 3B,C**). Based on the observations of i) more isoGDGT abundance at the northern SCS shelf in winter (e.g., roughly three times higher than in summer, Jia et al., 2017) and ii) its primary role (without contribution of terrigenous lipid input as represented by hopane contents, **Figure 4E**, and brGDGTs, **Supplementary Figure 1**) in regulating variations in the BIT index in our case, lower (higher) BIT values during the LIA (MCA) hence probably result from increased (decreased) production of the *Thaumarchaeota*, which is in good support of more (less) prevalence of wintertime conditions (Zhang et al., 2013; Wang et al., 2015; Jia et al., 2017). Combined with small BIT values downcore (roughly <0.3), terrigenous materials thus exert little (if any) impact on the TEX_{86} proxy (and its calibrated temperature). For the TEX_{86} thermometer, recent studies by Jia et al. (2017) and Wei et al. (2020) have also suggested that at the northern SCS coast, its estimates are commonly comparable to or slightly lower than winter SSTs, hence indicative of temperature signals in cold season (**Figure 2**). This interpretation, if true in our case, could explain the overall resemblance between our TEX_{86} values and the $U^{K'}_{37}$ SST record over the LIA (**Figure 3**), as it strongly indicates the homogeneity of thermal signals, in line with enhanced vertical mixing of onsite water due to a stronger AMC then. However, we still note that prior to the LIA interval, there existed slightly cooler (~0.5°C) values of TEX_{86} proxy during the MCA (**Figure 3**). Such observation, based on the winter temperature signals as earlier asserted (Jia et al., 2017; Wei et al., 2020), should necessitate a strengthening of winter AMC strength during the MCA (relative to the LIA), evidently contradicting not only our $U^{K'}_{37}$ SST and hopane records (Zhang et al., 2019) but also other terrestrial paleorecords (e.g., Yancheva et al., 2007; Kang et al., 2020). Therefore, additional parameter(s) must also be included here for completely understanding our TEX_{86} record.

In our case, downcore TEX_{86} values, calculated to be ~18.8 ± 1.2°C (**Figure 3C**, and roughly ~2°C higher if using regional equation developed by Jia et al., 2017), are obviously lower than the *in situ* instrumental SST in winter (**Figure 2**) considering that ~20% of *Thaumarchaeota* is actually produced in other seasons (Wang et al., 2015; Jia et al., 2017; Wei et al., 2020). Further, in light of i) its different features with the $U^{K'}_{37}$ SST record, ii) lower BIT values (<~0.3), and iii) use of the TEX_{86} proxy to manifest the temperature of subsurface rather than surface waters, for example, over the western Pacific marginal sea (Xing et al., 2015), we here apply TEX_{86} values as temperature indicators of an integrated water column but also biased toward winter season and subsurface waters (**Figure 2**). Although it is quite difficult to differentiate the inhabit depths of *Haptophyceae algae* (alkenone-producing species) and *Thaumarchaeota* at site YJ with ~21 m water depth, the use of $U^{K'}_{37}$- and TEX_{86}-derived temperatures to reflect the surface and subsurface thermal signals has been confirmed at the shallow water column in the northern SCS coast (e.g., ~50 m in Wang et al., 2021). Following such interpretation, within the LIA, an overall similarity in the temporal patterns of these two paired records (**Figure 3C** and **Figure 4A**) indicates the homogeneity of thermal signature down the entire water column here, thus calling for an intensification of vertical mixing due to a stronger winter AMC influence (Zhang et al., 2019). In contrast, during the MCA, a weaker winter AMC would have reduced vertical mixing which, together with a stronger summer AMC simultaneously (Dykoski et al., 2005; Zhang et al., 2008), intensified stratification of the water column and then eliminated the similar imprint of thermal conditions at different water depths, as extracted by $U^{K'}_{37}$-SST and TEX_{86} temperature records, respectively (**Figure 3C** and **Figure 4A**).

Since $U^{K'}_{37}$ mainly documents annual mean SST toward summer biases (Zhang et al., 2019) while the TEX_{86} index is largely controlled by winter temperature and the subsurface signal (**Figure 2**), the difference between our paired $U^{K'}_{37}$- and TEX_{86}-values, roughly ~6–7°C, can be used as a rough measure to represent thermal contrast at both seasonal and vertical scales (**Figure 4C**). As such, it shows that thermal gradient at the LIA was relatively small, for example, particularly down to ~4°C at a few short-lived epochs such as ~250 years BP, and ~500 years BP when the $U^{K'}_{37}$-SST record underwent abnormal cooling (of up ~4°C, **Figure 4A**), in comparison to that at the MCA (e.g., roughly ~8°C, **Figure 4C**). Together with similar variations of $U^{K'}_{37}$ and TEX_{86} records during the LIA, these multiple lines of independent evidence call for more influence of stronger AMC on the vertical mixing of subsurface water and thereby reduced stratification of the water column. Notably, considering the evolutionary role of winter AMC in regulating vertical mixing of subsurface waters at multi-centennial timescales, as discussed above, it is reasonable that, at our site YJ, the $U^{K'}_{37}$ – TEX_{86} gradient during the MCA is also likely amplified by an intensified stratification of the water column (and thus characterized by relatively larger errors) simultaneously. Reduction of vertical mixing, due to a weaker winter AMC (than during the LIA), would yield less influence of the subsurface cooling signal on surface temperature (generated by the $U^{K'}_{37}$ proxy, for example, Zhang et al., 2019). Water column stratification could also reshape *Euryarchaeota*/*Archaea* community and thus potentially drive TEX_{86} to lower values. This could have also contributed to the TEX_{86} values during the MCA, not particularly high as compared to the $U^{K'}_{37}$-SST values (**Figure 3C**). On the other hand, the TEX_{86} proxy well captures the temporal pattern of temperature changes within the LIA. Despite the potential contribution from *Euryarchaeota*/*Archaea* community changes, our calculation of vertical thermal gradient apparently resembles the temporal patterns of SST difference between the coast and open ocean (e.g., using $U^{K'}_{37}$-SST records at two sites YJ and NS02G, **Figure 4D**), whereas the SST difference is used to track winter AMC variability (Kong et al., 2017; Zhang et al., 2019). Assuming that the open sea SST represents "original"

temperature signal that is not strongly impacted by the winter AMC, the temperature difference between the two locations could indicate the winter AMC impact. The difference of our $U^{K'}_{37}$ and TEX_{86} values captures most of the features in the two $U^{K'}_{37}$-SST difference (**Figures 4C,D**), suggesting that the TEX_{86} proxy largely manifests the integrated water column/subsurface temperature at this site, despite its complicated nature. Hence, vertical thermal difference at the site YJ, associated with the strengthening (weakening) of onsite vertical mixing, facilitates our explanation of enhanced (reduced) winter AMC strength during the LIA (MCA). Altogether, secular changes in winter AMC intensity, for example, its intensification during the LIA, are capable of i) transporting terrigenous biomass, as substantiated by exponential increase of wind-borne hopane compounds (**Figure 4E**); ii) exerting additional cooling signals upon typical cold climate background (through both atmospheric and oceanic processes, Zhang et al., 2019), as seen by abnormal SST decrease (**Figure 4A**); and iii) enhancing vertical mixing (thereby reducing stratification) of the onsite water column, as reinforced by the similarity in $U^{K'}_{37}$ and TEX_{86} temperatures and decrease in their difference (**Figure 4C**), as well as lower BIT values.

CONCLUSION

We used a sediment core YJ, collected from the northern SCS coast, to analyze GDGT lipid biomarkers during the past millennium. These proxies, together with published alkenone ($U^{K'}_{37}$)-SST and hopane records from the same core, help constrain the dynamical interplay between northern SCS coastal conditions and winter AMC intensity at multi-centennial timescales. In general, variations in ACE and BIT indices, although characterized by opposite features, indicate a more prevalent regime of the winter season at the LIA (than the MCA). Further comparison of paired $U^{K'}_{37}$ and TEX_{86} temperature records, with the caution that the latter might be additionally affected by non-thermal factor, shows decrease (increase) in the vertical thermal gradient during the LIA (MCA), thereby calling for a well (less)-mixing of the onsite water column. Therefore, winter AMC changes would have greatly regulated both thermal and saline properties of the shallow waters at northern SCS coasts. Our results necessitate a careful examination of the AMC coupling processes for better understanding coastal environment in the past, for example, during the LIA and MCA, and also in the near future.

DATA AVAILABILITY STATEMENT

The original contributions presented in the study are included in the article/**Supplementary Material**; further inquiries can be directed to the corresponding author.

AUTHOR CONTRIBUTIONS

Conceptualization: ZL; investigation: KZ, CH, DK, YH, HW, and ZX; formal analysis: YZ and ZL; resources: WL, GW, and ZL; funding acquisition: WL and ZL; writing: YZ and ZL led the writing with intellectual contributions from all coauthors.

FUNDING

This work was supported by the National Key Research and Development Program of China (2016YFA0601204) and Hong Kong RGC Grant 17325516.

ACKNOWLEDGMENTS

We sincerely thank guest editors for inviting contribution to this special issue and anonymous referees for providing insightful comments to improve our manuscript.

SUPPLEMENTARY MATERIAL

The Supplementary Material for this article can be found online at: https://www.frontiersin.org/articles/10.3389/feart.2021.680180/full#supplementary-material

REFERENCES

An, Z., Clemens, S. C., Shen, J., Qiang, X., Jin, Z., Sun, Y., et al. (2011). Glacial-interglacial Indian Summer Monsoon Dynamics. *Science* 333, 719–723. doi:10.1126/science.1203752

Blaauw, M., and Christen, J. A. (2011). Flexible Paleoclimate Age-Depth Models Using an Autoregressive Gamma Process. *Bayesian Anal.* 6, 457–474. doi:10.1214/ba/1339616472

Bollasina, M. A., Ming, Y., and Ramaswamy, V. (2011). Anthropogenic Aerosols and the Weakening of the South Asian Summer Monsoon. *Science* 334, 502–505. doi:10.1126/science.1204994

Cai, W., Wu, L., Lengaigne, M., Li, T., McGregor, S., Kug, J.-S., et al. (2019). Pantropical Climate Interactions. *Science* 363, eaav4236. doi:10.1126/science.aav4236

Casey, K. (2013). *US DOC/NOAA/NESDIS > National Oceanographic Data Center, AVHRR Pathfinder Version 5.0 Global 4km Sea Surface Temperature (SST) Cloud-Screened Monthly Climatologies for 1985-2006 (NODC Accession 0110657)*. NOAA: National Oceanographic Data Center.

Cheng, H., Edwards, R. L., Sinha, A., Spötl, C., Yi, L., Chen, S., et al. (2016). The Asian Monsoon over the Past 640,000 Years and Ice Age Terminations. *Nature* 534 (7609), 640–646. doi:10.1038/nature18591

Dunn, J. R., and Ridgway, K. R. (2002). Mapping Ocean Properties in Regions of Complex Topography. *Deep Sea Res. Oceanographic Res. Pap.* 49 (3), 591–604. doi:10.1016/s0967-0637(01)00069-3

Dykoski, C., Edwards, R., Cheng, H., Yuan, D., Cai, Y., Zhang, M., et al. (2005). A High-Resolution, Absolute-Dated Holocene and Deglacial Asian Monsoon Record from Dongge Cave, China. *Earth Planet. Sci. Lett.* 233, 71–86. doi:10.1016/j.epsl.2005.01.036

He, Y., Wang, H., Meng, B., Liu, H., Zhou, A., Song, M., et al. (2020). Appraisal of Alkenone- and Archaeal Ether-Based Salinity Indicators in Mid-latitude Asian Lakes. *Earth Planet. Sci. Lett.* 538, 116236. doi:10.1016/j.epsl.2020.116236

Hopmans, E. C., Weijers, J. W. H., Schefuss, E., Herfort, L., Sinninghe Damsté, J. S., and Schouten, S. (2004). A Novel Proxy for Terrestrial Organic Matter in

Sediments Based on Branched and Isoprenoid Tetraether Lipids. *Earth Planet. Sci. Lett.* 224, 107–116. doi:10.1016/j.epsl.2004.05.012

Hu, C., Henderson, G. M., Huang, J., Xie, S., Sun, Y., and Johnson, K. R. (2008). Quantification of Holocene Asian Monsoon Rainfall from Spatially Separated Cave Records. *Earth Planet. Sci. Lett.* 266, 221–232. doi:10.1016/j.epsl.2007.10.015

Huang, C., Zeng, T., Ye, F., Xie, L., Wang, Z., Wei, G., et al. (2018). Natural and Anthropogenic Impacts on Environmental Changes over the Past 7500 Years Based on the Multi-Proxy Study of Shelf Sediments in the Northern South China Sea. *Quat. Sci. Rev.* 197, 35–48. doi:10.1016/j.quascirev.2018.08.005

Huang, E., Tian, J., and Steinke, S. (2011). Millennial-scale Dynamics of the winter Cold Tongue in the Southern South China Sea over the Past 26 Ka and the East Asian winter Monsoon. *Quat. Res.* 75, 196–204. doi:10.1016/j.yqres.2010.08.014

Huguet, C., Hopmans, E. C., Febo-Ayala, W., Thompson, D. H., Sinninghe Damsté, J. S., and Schouten, S. (2006). An Improved Method to Determine the Absolute Abundance of Glycerol Dibiphytanyl Glycerol Tetraether Lipids. *Org. Geochem.* 37, 1036–1041. doi:10.1016/j.orggeochem.2006.05.008

Jia, G., Wang, X., Guo, W., and Dong, L. (2017). Seasonal Distribution of Archaeal Lipids in Surface Water and its Constraint on Their Sources and the TEX86 Temperature Proxy in Sediments of the South China Sea. *J. Geophys. Res. Biogeosci.* 122, 592–606. doi:10.1002/2016jg003732

Jing, Z.-y., Qi, Y.-q., Hua, Z.-l., and Zhang, H. (2009). Numerical Study on the Summer Upwelling System in the Northern continental Shelf of the South China Sea. *Continental Shelf Res.* 29, 467–478. doi:10.1016/j.csr.2008.11.008

Kang, S., Du, J., Wang, N., Dong, J., Wang, D., Wang, X., et al. (2020). Early Holocene Weakening and Mid- to Late Holocene Strengthening of the East Asian winter Monsoon. *Geology* 48 (11), 1043–1047. doi:10.1130/g47621.1

Kim, J.-H., van der Meer, J., Schouten, S., Helmke, P., Willmott, V., Sangiorgi, F., et al. (2010). New Indices and Calibrations Derived from the Distribution of Crenarchaeal Isoprenoid Tetraether Lipids: Implications for Past Sea Surface Temperature Reconstructions. *Geochimica et Cosmochimica Acta* 74, 4639–4654. doi:10.1016/j.gca.2010.05.027

Kok, J. F., Ward, D. S., Mahowald, N. M., and Evan, A. T. (2018). Global and Regional Importance of the Direct Dust-Climate Feedback. *Nat. Commun.* 9, 241. doi:10.1038/s41467-017-02620-y

Kong, D. (2014a). *Climatic Changes in the Northern South China Sea since the Last Glacial Maximum. PhD Thesis*. Hong Kong: University of Hong Kong. doi:10.5353/th_b5312314

Kong, D., Wei, G., Chen, M.-T., Peng, S., and Liu, Z. (2017). Northern South China Sea SST Changes over the Last Two Millennia and Possible Linkage with Solar Irradiance. *Quat. Int.* 459, 29–34. doi:10.1016/j.quaint.2017.10.001

Kong, D., Zong, Y., Jia, G., Wei, G., Chen, M.-T., and Liu, Z. (2014b). The Development of Late Holocene Coastal Cooling in the Northern South China Sea. *Quat. Int.* 349, 300–307. doi:10.1016/j.quaint.2013.08.055

Lau, N.-C., and Nath, M. J. (2009). A Model Investigation of the Role of Air-Sea Interaction in the Climatological Evolution and ENSO-Related Variability of the Summer Monsoon over the South China Sea and Western North Pacific. *J. Clim.* 22, 4771–4792. doi:10.1175/2009jcli2758.1

Lee, W.-M., Poon, K.-C., Kong, D., Sewell, R. J., Zong, Y., Zhang, Y., et al. (2019). Summer Monsoon-Induced Upwelling Dominated Coastal Sea Surface Temperature Variations in the Northern South China Sea over the Last Two Millennia. *The Holocene* 29 (4), 691–698. doi:10.1177/0959683618824715

Li, Y., and Morrill, C. (2015). A Holocene East Asian winter Monsoon Record at the Southern Edge of the Gobi Desert and its Comparison with a Transient Simulation. *Clim. Dyn.* 45, 1219–1234. doi:10.1007/s00382-014-2372-5

Li, Z., Lau, W. K. M., Ramanathan, V., Wu, G., Ding, Y., Manoj, M. G., et al. (2016). Aerosol and Monsoon Climate Interactions over Asia. *Rev. Geophys.* 54, 866–929. doi:10.1002/2015rg000500

Liu, B., and Zhu, C. (2016). A Possible Precursor of the South China Sea Summer Monsoon Onset: Effect of the South Asian High. *Geophys. Res. Lett.* 43, 11072–11079. doi:10.1002/2016gl071083

Liu, J., Chen, J., Zhang, X., Li, Y., Rao, Z., and Chen, F. (2015). Holocene East Asian Summer Monsoon Records in Northern China and Their Inconsistency with Chinese Stalagmite δ18O Records. *Earth-Science Rev.* 148, 194–208. doi:10.1016/j.earscirev.2015.06.004

Liu, W., Wang, H., Zhang, C. L., Liu, Z., and He, Y. (2013). Distribution of Glycerol Dialkyl Glycerol Tetraether Lipids along an Altitudinal Transect on Mt. Xiangpi, NE Qinghai-Tibetan Plateau, China. *Org. Geochem.* 57, 76–83. doi:10.1016/j.orggeochem.2013.01.011

Maher, B. A., Prospero, J. M., Mackie, D., Gaiero, D., Hesse, P. P., and Balkanski, Y. (2010). Global Connections between Aeolian Dust, Climate and Ocean Biogeochemistry at the Present Day and at the Last Glacial Maximum. *Earth-Science Rev.* 99, 61–97. doi:10.1016/j.earscirev.2009.12.001

Mann, M. E., Zhang, Z., Hughes, M. K., Bradley, R. S., Miller, S. K., Rutherford, S., et al. (2008). Proxy-based Reconstructions of Hemispheric and Global Surface Temperature Variations over the Past Two Millennia. *Proc. Natl. Acad. Sci.* 105 (36), 13252–13257. doi:10.1073/pnas.0805721105

Prahl, F. G., Muehlhausen, L. A., and Zahnle, D. L. (1988). Further Evaluation of Long-Chain Alkenones as Indicators of Paleoceanographic Conditions. *Geochimica et Cosmochimica Acta* 52, 2303–2310. doi:10.1016/0016-7037(88)90132-9

Reimer, P. J., Bard, E., Bayliss, A., Beck, J. W., Blackwell, P. G., Ramsey, C. B., et al. (2013). IntCal13 and Marine13 Radiocarbon Age Calibration Curves 0-50,000 Years Cal BP. *Radiocarbon* 55, 1869–1887. doi:10.2458/azu_js_rc.55.16947

Schouten, S., Hopmans, E. C., Schefuss, E., and Sinninghe Damsté, J. S. (2002). Distributional Variations in marine Crenarchaeotal Membrane Lipids: a New Tool for Reconstructing Ancient Sea Water Temperatures? *Earth Planet. Sci. Lett.* 204, 265–274. doi:10.1016/s0012-821x(02)00979-2

Schouten, S., Hopmans, E. C., and Sinninghe Damsté, J. S. (2013). The Organic Geochemistry of Glycerol Dialkyl Glycerol Tetraether Lipids: a Review. *Org. Geochem.* 54, 19–61. doi:10.1016/j.orggeochem.2012.09.006

Southon, J., Kashgarian, M., Fontugne, M., Metivier, B., and W-S Yim, W. (2002). Marine Reservoir Corrections for the Indian Ocean and Southeast Asia. *Radiocarbon* 44, 167–180. doi:10.1017/s0033822200064778

Steinke, S., Glatz, C., Mohtadi, M., Groeneveld, J., Li, Q., and Jian, Z. (2011). Past Dynamics of the East Asian Monsoon: No Inverse Behaviour between the Summer and winter Monsoon during the Holocene. *Glob. Planet. Change* 78, 170–177. doi:10.1016/j.gloplacha.2011.06.006

Stevens, T., Thomas, D., Armitage, S., Lunn, H., and Lu, H. (2007). Reinterpreting Climate Proxy Records from Late Quaternary Chinese Loess: A Detailed OSL Investigation. *Earth-Science Rev.* 80, 111–136. doi:10.1016/j.earscirev.2006.09.001

Tian, J., Huang, E., and Pak, D. K. (2010). East Asian winter Monsoon Variability over the Last Glacial Cycle: Insights from a Latitudinal Sea-Surface Temperature Gradient across the South China Sea. *Palaeogeogr. Palaeoclimatol. Palaeoecol.* 292, 319–324. doi:10.1016/j.palaeo.2010.04.005

Turich, C., and Freeman, K. (2011). Archaeal Lipids Record Paleosalinity in Hypersaline Systems. *Org. Geochem.* 42, 1147–1157.

Turich, C., Freeman, K., Freeman, K. H., Bruns, M. A., Conte, M., Jones, A. D., et al. (2007). Lipids of marine Archaea: Patterns and Provenance in the Water-Column and Sediments. *Geochimica et Cosmochimica Acta* 71, 3272–3291. doi:10.1016/j.gca.2007.04.013

Wang, B., Huang, F., Wu, Z., Yang, J., Fu, X., and Kikuchi, K. (2009). Multi-scale Climate Variability of the South China Sea Monsoon: A Review. *Dyn. Atmospheres Oceans* 47, 15–37. doi:10.1016/j.dynatmoce.2008.09.004

Wang, H., Liu, W., Zhang, C. L., Jiang, H., Dong, H., Lu, H., et al. (2013). Assessing the Ratio of Archaeol to Caldarchaeol as a Salinity Proxy in highland Lakes on the Northeastern Qinghai-Tibetan Plateau. *Org. Geochem.* 54, 69–77. doi:10.1016/j.orggeochem.2012.09.011

Wang, J.-X., Wei, Y., Wang, P., Hong, Y., and Zhang, C. L. (2015). Unusually Low TEX86 Values in the Transitional Zone between Pearl River Estuary and Coastal South China Sea: Impact of Changing Archaeal Community Composition. *Chem. Geology.* 402, 18–29. doi:10.1016/j.chemgeo.2015.03.002

Wang, L., Li, J., Lu, H., Gu, Z., Rioual, P., Hao, Q., et al. (2012). The East Asian winter Monsoon over the Last 15,000 Years: its Links to High-Latitudes and Tropical Climate Systems and Complex Correlation to the Summer Monsoon. *Quat. Sci. Rev.* 32, 131–142. doi:10.1016/j.quascirev.2011.11.003

Wang, M., Wang, H., Zhu, Z., Yang, X., Zhang, K., Zhang, Y., et al. (2021). Late Miocene-Pliocene Asian Summer Monsoon Variability Linked to Both Tropical Pacific Temperature and Walker Circulation. *Earth Planet. Sci. Lett.* 561 (116823), 116823. doi:10.1016/j.epsl.2021.116823

Wang, P. X., Wang, B., Cheng, H., Fasullo, J., Guo, Z., Kiefer, T., et al. (2017). The Global Monsoon across Time Scales: Mechanisms and Outstanding Issues. *Earth-Science Rev.* 174, 84–121. doi:10.1016/j.earscirev.2017.07.006

Wang, Y., Cheng, H., Edwards, R., He, Y., Kong, X., An, Z., et al. (2005). The Holocene Asian Monsoon: Links to Solar Changes and North Atlantic Climate. *Science* 308, 854–857. doi:10.1126/science.1106296

Wei, B., Jia, G., Hefter, J., Kang, M., Park, E., Wang, S., et al. (2020). Comparison of the U37K′, LDI, TEX86H, and RI-OH Temperature Proxies in Sediments from the Northern Shelf of the South China Sea. *Biogeosciences* 17, 4489–4508. doi:10.5194/bg-17-4489-2020

Weijers, J. W. H., Schefuß, E., Kim, J.-H., Sinninghe Damsté, J. S., and Schouten, S. (2014). Constraints on the Sources of Branched Tetraether Membrane Lipids in Distal marine Sediments. *Org. Geochem.* 72, 14–22. doi:10.1016/j.orggeochem.2014.04.011

Wen, X., Liu, Z., Wang, S., Cheng, J., and Zhu, J. (2016). Correlation and Anti-correlation of the East Asian Summer and winter Monsoons during the Last 21,000 Years. *Nat. Commun.* 7. doi:10.1038/ncomms11999

W. Wang (2007). *Study on the Coastal Geomorphological Sedimentation of the South China Sea* (Guangzhou, China: Guangdong Economy Publishing House), 344 in Chinese.

Xiao, W., Wang, Y., Zhou, S., Hu, L., Yang, H., and Xu, Y. (2016). Ubiquitous Production of Branched Glycerol Dialkyl Glycerol Tetraethers (brGDGTs) in Global marine Environments: a New Source Indicator for brGDGTs. *Biogeosciences* 13, 5883–5894. doi:10.5194/bg-13-5883-2016

Xie, A., Chung, Y., Liu, X., and Ye, Q. (1998). The Interannual Variations of Summer Monsoon Onset Over the South China Sea. *Theor. Appl. Climatol.* 59, 201–213.

Xie, S.-P., Deser, C., Vecchi, G. A., Collins, M., Delworth, T. L., Hall, A., et al. (2015). Towards Predictive Understanding of Regional Climate Change. *Nat. Clim Change* 5, 921–930. doi:10.1038/nclimate2689

Xing, L., Sachs, J. P., Gao, W., Tao, S., Zhao, X., Li, L., et al. (2015). TEX 86 Paleothermometer as an Indication of Bottom Water Temperature in the Yellow Sea. *Org. Geochem.* 86, 19–31. doi:10.1016/j.orggeochem.2015.05.007

Yamamoto, M., Kishizaki, M., Oba, T., and Kawahata, H. (2013). Intense winter Cooling of the Surface Water in the Northern Okinawa Trough during the Last Glacial Period. *J. Asian Earth Sci.* 69, 86–92. doi:10.1016/j.jseaes.2012.06.011

Yancheva, G., Nowaczyk, N. R., Mingram, J., Dulski, P., Schettler, G., Negendank, J. F. W., et al. (2007). Influence of the Intertropical Convergence Zone on the East Asian Monsoon. *Nature* 445, 74–77. doi:10.1038/nature05431

Yu, K., Hua, Q., Zhao, J.-x., Hodge, E., Fink, D., and Barbetti, M. (2010). Holocene marine14C Reservoir Age Variability: Evidence from230Th-Dated Corals in the South China Sea. *Paleoceanography* 25. doi:10.1029/2009PA001831

Zhang, C., Tang, Q., Chen, D., Li, L., Liu, X., and Cui, H. (2017). Tracing Changes in Atmospheric Moisture Supply to the Drying Southwest China. *Atmos. Chem. Phys.* 17, 10383–10393. doi:10.5194/acp-17-10383-2017

Zhang, J., Bai, Y., Xu, S., Lei, F., and Jia, G. (2013). Alkenone and Tetraether Lipids Reflect Different Seasonal Seawater Temperatures in the Coastal Northern South China Sea. *Org. Geochem.* 58, 115–120. doi:10.1016/j.orggeochem.2013.02.012

Zhang, P., Cheng, H., Edwards, R. L., Chen, F., Wang, Y., Yang, X., et al. (2008). A Test of Climate, Sun, and Culture Relationships from an 1810-year Chinese Cave Record. *Science* 322, 940–942. doi:10.1126/science.1163965

Zhang, Y., Zhu, K., Huang, C., Kong, D., He, Y., Wang, H., et al. (2019). Asian winter Monsoon Imprint on Holocene SST Changes at the Northern Coast of the South China Sea. *Geophys. Res. Lett.* 46, 13363–13370. doi:10.1029/2019gl085617

Zhu, C., Wakeham, S. G., Elling, F. J., Basse, A., Mollenhauer, G., Versteegh, G. J. M., et al. (2016). Stratification of Archaeal Membrane Lipids in the Ocean and Implications for Adaptation and Chemotaxonomy of Planktonic Archaea. *Environ. Microbiol.* 18, 4324–4336. doi:10.1111/1462-2920.13289

Zweng, M., Reagan, J., Antonov, J., Locarnini, R., Mishonov, A., Boyer, T., et al. (2013). "World Ocean Atlas," in *NOAA Atlas NESDIS*. Editors S. L. Salinity and A. Mishonov, 39.

Conflict of Interest: The authors declare that the research was conducted in the absence of any commercial or financial relationships that could be construed as a potential conflict of interest.

The reviewer (YH) declared a shared affiliation with several of the authors, (HW, WL, ZX), to the handling editor at time of review.